View Online
Dynamic Article Links

Dalton Transactions

Cite this: *Dalton Trans.*, 2011, **40**, 6738

www.rsc.org/dalton

PAPER

Interplay between structure, stoichiometry and properties of technetium nitrides

Philippe F. Weck,*[a] Eunja Kim[b] and Kenneth R. Czerwinski[a]

Received 26th February 2011, Accepted 13th April 2011
DOI: 10.1039/c1dt10334b

We report first-principles calculations of the structures and properties of technetium nitride phases within the framework of gradient-corrected density functional theory. Specifically, we have investigated the possible existence of hexagonal Tc_3N and Tc_2N subnitrides, following the recent discovery of Re nitrides analogues synthesized directly from the elements. These novel Tc subnitride phases, which are predicted to be stable, are also compared with bulk Tc and Tc mononitride in order to shed light on the intrinsic relationships between the structure, Tc/N stoichiometry, and properties in the Tc–N system.

Introduction

Transition-metal (TM) nitrides have received increasing theoretical and experimental attention owing to their outstanding mechanical, thermal, optoelectronic, semiconducting, magnetic or superconducting properties, which can be used advantageously in a variety of technological applications.[1–5] Although the intercalation of small covalent atoms such as nitrogen into transition metals is a well-established strategy for designing materials with high hardness and melting point,[6] recent advances in the synthesis of TM nitrides have opened up new avenues of research.[7–11]

Most of the research effort on binary TM nitrides has been focused so far on alloys composed of groups IV–VI metals, in which N atoms tend to occupy interstitial sites, with a marked propensity to form non-stoichiometric compounds.[12] Recently, considerable work has also been devoted to the investigation of binary nitrides of groups VIII–X noble transition metals with the general formula MN_2 (M = Os, Ir, Pt, Ru, Rh, Pd).[7–9,11,13] This contrasts with the scarcity of knowledge available on binary nitrides of group VII metals, in particular on the characterization of crystalline phases of rhenium nitride[10,14–19] and technetium nitride.[20,21]

This lack of information on Tc–N phases appears especially surprising in light of the importance of technetium in the fields of nuclear waste management and nuclear medicine. Although technetium possesses no stable isotopes, its longlived β^-–emitting isotope, ^{99}Tc ($t_{1/2}$ = 2.13 × 10^5 years, β^- = 294 keV), is produced in sizeable amounts from the nuclear fuel cycle (up to 6% fission yield) and constitutes an important challenge for environmental remediation.[22,23] In this context, the development of potential Tc-rich nitride waste forms with bulk moduli and melting temperatures significantly higher than bulk Tc, and with high chemical stability and corrosion resistance, is of particular interest. Additionally, ^{99m}Tc, the short–lived γ–emitting isotope of technetium originating from the decay of ^{99}Mo, is the most common isotope in diagnostic nuclear medicine (*ca.* 85% of all procedures) due to its optimal nuclear properties as a radioimaging agent ($t_{1/2}$ = 6.02 h, γ = 142 keV) and ^{99m}Tc nitrido complexes constitute an important class of radiopharmaceuticals.[24–28]

Experimentally, it was suggested that technetium nitrides can be synthesized by hydrogen reduction of NH_4TcO_4 in ammonia at 900–1100 °C or by thermal decomposition of $(NH_4)_2[TcCl_6]$ or $(NH_4)_2[TcBr_6]$ at 380 °C under argon atmosphere. The phases investigated experimentally were found to crystallize in the face-centered-cubic (FCC) structure with a lattice constant varying from 3.980 to 3.985 Å, depending on the amount of nitrogen absorbed, and with a maximum nitrogen content approximated to the composition $TcN_{0.76}$.[20,21]

On the theoretical side, calculations performed to date on binary technetium nitrides have been limited to perfect stoichiometric TcN crystals, to the best of our knowledge.[29,30] Early cohesive energy calculations carried out by Fernández–Guillermet and coworkers using the linear muffin-tin orbital (LMTO) method were restricted to Tc mononitride in the NaCl-type structure.[29] Subsequent full-potential linearized augmented plane-wave (FLAPW) calculations by de Paiva *et al.* investigated the electronic structure of zincblende-type TcN.[30] Although only TcN has been investigated so far, other crystal structures with Tc_2N, Tc_4N or TcN_2 stoichiometries are predicted to exist since Hägg's rule is fulfilled,[31] *i.e.* $R_N/R_{Tc} < 0.59$, where R_N and R_{Tc} are the atomic radii of N and Tc, respectively. In practice, the phases can actually exhibit a larger variety of compositions depending on the synthetic pathways followed.

In this study, we report first-principles calculations of the structure, stability and properties of technetium nitride phases within the framework of gradient-corrected density functional theory (DFT). Specifically, we have investigated the possible

[a]*Department of Chemistry, University of Nevada-Las Vegas, Las Vegas, NV, 89154, USA. E-mail: weckp@unlv.nevada.edu; Fax: (702) 895-4072; Tel: (702) 895-1159*
[b]*Department of Physics and Astronomy, University of Nevada-Las Vegas, Las Vegas, NV, 89154, USA*

Table 1 Calculated equilibrium lattice parameters (a, in Å), axial ratio (c/a), zero-pressure elastic constants (C_{ij}, in GPa), Voigt, Reuss, and Hill bulk moduli (B_V, B_R, and B, in GPa), Voigt, Reuss, and Hill shear moduli (G_V, G_R, and G, in GPa), Young's modulus (E, in GPa), Poisson's ratio (ν), and compressibility (β, in 1/GPa)

	Tc				TcN				
	*P*6$_3$/*mmc*	Expt.	Tc_3N *P*-6*m*2	Tc_2N *P*6$_3$/*mmc*	*F*-43*m*	*P*6$_3$*mc*	*P*6$_3$/*mmc*	*P*-6*m*2	*Fm*-3*m*
a	2.75[a]	2.7409[c]	2.83[a]	2.85[a]	4.60[a]	3.23[a]	2.83[a]	2.84[a]	4.33[a]
	2.76[b]		2.84[b]	2.87[b]	4.62[b]	3.27[b]	2.89[b]	2.84[b]	4.35[b]
c/a	1.60[a]	1.6048[c]	2.50[a]	3.42[a]		1.67[a]	2.00[a]	1.01[a]	
	1.60[b]		2.50[b]	3.40[b]		1.65[b]	1.94[b]	1.03[b]	
C_{11}	478	433[d]	495	499	300	233	492	456	468
C_{33}	480	470[d]	597	564		394	714	621	
C_{44}	131	117[d]	151	147	−12	−28	175	−15	−187
C_{12}	198	199[d]	189	159	243	307	197	225	246
C_{13}	212	199[d]	229	278		192	260	268	
B_V	298		320	333	262	249	349	340	320
B_R	298		315	321	262	249	334	329	320
B	298	281[d]	318	327	262	249	341	334	320
G_V	134		153	149			170		
G_R	134		153	144			166		
G	134	119[d]	153	147			167		
E	350	314[d]	396	384			431		
ν	0.30	0.31[d]	0.29	0.30			0.29		
β	0.0034	0.0036[d]	0.0032	0.0031	0.0038	0.0040	0.0030	0.0030	0.0031

[a] This work, VASP. [b] This work, CASTEP. [c] Ref.[32] [d] Ref.[36]

existence of hexagonal Tc_3N and Tc_2N subnitrides, following the recent discovery of Re nitrides analogues synthesized directly from the elements.[10] These Tc subnitride phases, which are predicted to be stable, are also compared with bulk Tc and Tc mononitride in order to shed light on the intrinsic relationships between the structure, Tc/N stoichiometry and properties in the Tc–N system.

A complete discussion of our results is given in the next section, followed by a summary of our findings and conclusions. Details of our computational approach are given in the last section of the manuscript.

Results and discussion

Crystal structures and formation

Optimized geometries of the crystal unit cells of bulk Tc (space group *P*6$_3$/*mmc*), Tc_3N (space group *P*$\bar{6}$*m*2), Tc_2N (space group *P*6$_3$/*mmc*) and TcN (space group *P*6$_3$/*mmc*) computed at the GGA/PW91 level of theory are displayed in Fig. 1. For bulk Tc, the lowest-energy structure corresponds to the HCP atomic arrangement with calculated lattice parameters of a = 2.75 Å and c = 4.40 Å with VASP and 2.76 Å and c = 4.42 with CASTEP, in close agreement with the experimental values of a_0 = 2.7409 ± 0.0035 Å and c_0 = 4.3987 ± 0.0034 Å at ambient temperature and pressure.[32] As shown in Fig. 2 representing the variation of the total energy of bulk Tc as a function of the volume per atom, the FCC structure for Tc metal is slightly less energetically favorable than the HCP structure. The FCC lattice parameter calculated with VASP is a = 3.87 Å, close to the experimental value of a_0 = 3.68 Å for polycrystalline films thinner than 15 nm which adopt the FCC structure.[33] Other atomic arrangements such as the simple cubic (SC) and body-centered cubic (BCC) structures were also investigated for bulk Tc but were found to be energetically unfavorable. From Fig. 2, we can also infer that no pressure-induced phase transition is likely to occur in Tc metal, consistent with experimental findings.[34] For Tc_3N, the optimized structure crystallizing in the *P*$\bar{6}$*m*2 space group [Tc at Wyckoff positions 1*f* and 2*h* with z = 0.197, N at 1*e*] features an equilibrium lattice parameter of a = 2.83 Å and an axial ratio of c/a = 2.50 with VASP. For Tc_2N with the *P*6$_3$/*mmc* symmetry [Tc at Wyckoff positions 4*f* with z = 0.108, N at 2*d*], the equilibrium lattice parameter and axial ratio computed with VASP are a = 2.85 Å and c/a = 3.42, respectively. The variation of the total energy of Tc_3N and Tc_2N as a function of the volume per atom is represented in Fig. 3(a)–(b). For Tc mononitride, the zincblende-type ZnS (*F*$\bar{4}$3*m*, a = 4.60 Å) structure is predicted to be the most energetically favorable phase, followed by the NiAs (*P*6$_3$/*mmc*, a = 2.83 Å and c/a = 2.00), wurtzite-type ZnS (*P*6$_3$*mc*, a = 3.23 Å and c/a = 1.67), WC (*P*$\bar{6}$*m*2, a = 2.84 Å and c/a = 1.01), and NaCl (*Fm*$\bar{3}$*m*, a = 4.33 Å) structures [*cf.* Fig. 3 (c)]. It is interesting to note that the zincblende structure is also energetically more preferable for ReN.[19] As shown in Table 1, structural parameters of the model phases relaxed with CASTEP are in close agreement with VASP results discussed above.

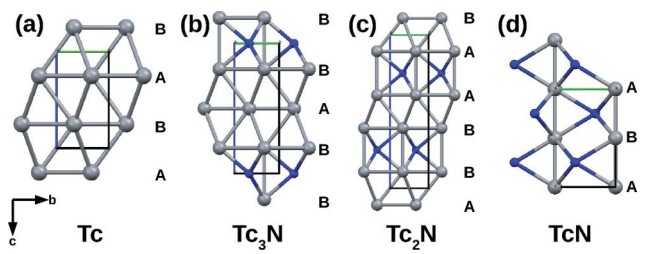

Fig. 1 Ball-and-stick models of the stable crystal structures of (a) bulk Tc (space group *P*6$_3$/*mmc*, Z = 2), (b) Tc_3N (space group *P*$\bar{6}$*m*2, Z = 1), (c) Tc_2N (space group *P*6$_3$/*mmc*, Z = 2) and (d) TcN (space group *P*6$_3$/*mmc*, Z = 2) optimized at the GGA/PW91 level of theory. Color legend: N, navy blue; Tc, grey.

For the sake of comparison with the FCC $TcN_{0.76}$ phase observed experimentally, a model rocksalt $TcN_{0.75}$ unit cell with

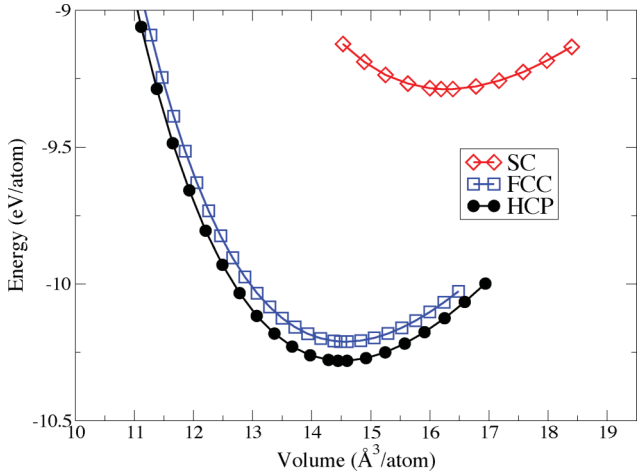

Fig. 2 Variation of the total energy of bulk Tc as a function of the volume per atom calculated at the GGA/PW91 level for hexagonal close-packed (HCP), face-centered cubic (FCC) and simple cubic (SC) unit cells.

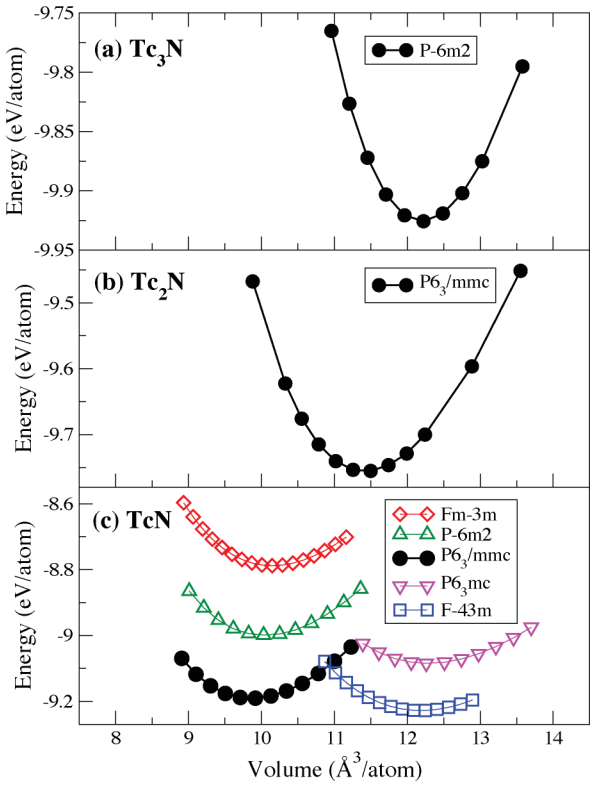

Fig. 3 Variation of the total energy of (a) Tc_3N, (b) Tc_2N and (c) TcN as a function of the volume per atom calculated at the GGA/PW91 level. For TcN, the energy variation for NaCl ($Fm\bar{3}m$), NiAs ($P6_3/mmc$), WC ($P\bar{6}m2$), zincblende ($F\bar{4}3m$) and wurtzite ($P6_3mc$) structures are depicted.

a central N vacancy was relaxed using VASP. The resulting equilibrium lattice parameter is $a = 4.24$ Å, *i.e.* 2% shorter than the ideal NaCl-type TcN phase, but significantly larger than the value of 3.980–3.985 Å reported experimentally.[20,21] Although further experimental effort is needed to resolve this discrepancy, this lattice contraction with respect to the calculated parameter suggests that more defects might actually exist in the sample characterized as $TcN_{0.76}$. Indeed, our calculations predict that the N vacancy formation energy in the FCC TcN unit cell, *i.e.* $E_f(N_{vac}) = E_{tot}^{TcN} - E_{tot}^{TcN_{0.75}} - (1/2)E_{tot}^{N_2(g)}$, is +1.78 eV, and therefore the formation of defective Tc subnitride compounds is energetically more favorable than the formation of perfect stoichiometric Tc mononitride.

The enthalpy of formation of crystalline Tc nitrides calculated in the athermal limit using eqn (2) is $\Delta H_f = -0.50$ eV/f.u. for Tc_3N and −0.38 eV/f.u. for Tc_2N, with a negative value corresponding to an exothermic reaction. For all the candidate TcN structures investigated the formation reaction is endothermic (+0.18, +0.26, +0.47, +0.64, and +1.06 eV/f.u. for the $F\bar{4}3m$, $P6_3/mmc$, $P6_3mc$, $P\bar{6}m2$, and $Fm\bar{3}m$ structures, respectively). However, this does not preclude the possibility that TcN formation might occur at high temperature and/or pressure. These results reveal a propensity of the Tc–N system to form Tc-rich phases.

Mechanical properties

In addition to the phase stability requirement based on energetic considerations, the criteria formulated by Born and Huang[35] in terms of the elastic constants, C_{ij}, must be satisfied to insure complete mechanical stability of the crystalline phases. The mechanical stability of a cubic crystal requires that the elastic constants obey the relations $C_{11} - C_{12} > 0$, $C_{11} + 2C_{12} > 0$ and $C_{44} > 0$, and for a hexagonal crystal, $C_{11} > 0$, $C_{33} > 0$, $C_{44} > 0$, $C_{66} > 0$, $C_{11} - C_{12} > 0$, $C_{11} + C_{12} + C_{33} > 0$, and $(C_{11} + C_{12})C_{33} - 2C^2_{13} > 0$. The values of the C_{ij} coefficients for bulk Tc, Tc_3N, Tc_2N, and TcN crystals calculated at the GGA/PW91 level of theory are given in Table 1. For Tc bulk, the computed elastic constants are in fair agreement with experimental values derived from the phonon dispersion curves measured by neutron scattering and the computed bulk modulus is ≈ 6% larger than the experimental value of 281 GPa obtained from sound velocity data.[36] The calculated elastic constants of bulk Tc ($P6_3/mmc$), Tc_3N ($P\bar{6}m2$), Tc_2N ($P6_3/mmc$) and TcN ($P6_3/mmc$) phases fulfil all the mechanical stability criteria for hexagonal crystals. However, none of the other candidate structures proposed for TcN satisfies the $C_{44} > 0$ condition. Interestingly, the zincblende structure was also predicted to be mechanically unstable for ReN, although it is energetically more preferable.[19,37] The inferior mechanical properties of the zincblende and wurtzite structures of TcN, which possess the smallest bulk moduli among the candidate TcN phases (*i.e.* 262 GPa for $F\bar{4}3m$ and 249 GPa for $P6_3mc$), may be ascribed in part to their large volume per formula unit.

The C_{11} and C_{33} elastic constants, which correspond to the resistance to linear compression along the *x* and *z* crystallographic axes, are larger for Tc nitrides compared to bulk Tc. While C_{11} varies only by ≈ 4% with increasing N content, the largest variation appears for C_{33} which increases from 480 GPa for bulk Tc to 714 GPa for the stable $P6_3/mmc$ TcN phase. This might be the result of the peculiar structure of Tc–N lattices with alternating Tc and N layers along the *z* direction, *i.e.* with *ABB*, *AABB* and *ABAB* stacking sequences of Tc atoms in the unit cells of Tc_3N, Tc_2N and $P6_3/mmc$ TcN, respectively (*cf.* Fig. 1). In order to assess the elastic anisotropy of these compounds, we used the shear anisotropic factor $A(C_{ij})$, defined as $A = 4C_{44}/(C_{11} + C_{33} - 2C_{13})$ for the {100} shear planes between the <011> and <010> directions,[38] as well as the ratio between linear compressibility coefficients for hexagonal crystals, *i.e.* $k_c/k_a = (C_{11} + C_{12} - 2C_{13})/(C_{33} - C_{13})$. The computed shear anisotropic factors are 0.95, 1.16 and 1.02 for the Tc_3N,

Tc_2N and $P6_3/mmc$ TcN structures, appreciably departing from the value of 0.98 for Tc metal. In addition, while bulk Tc exhibits a nearly isotropic compressibility with a k_c/k_a ratio of 0.94, the Tc_3N (0.61), Tc_2N (0.36), and the $P6_3/mmc$ TcN (0.37) phases show rather anisotropic c/a compressibility. In terms of the recently introduced universal anisotropy index,[39] $A^U = 5(G_V/G_R) + (B_V/B_R) - 6$, bulk Tc can be considered as a perfectly isotropic crystal (A^U = 0.00), unlike Tc_3N (0.02), Tc_2N (0.21), and $P6_3/mmc$ TcN (0.16).

As shown in Table 1, the computed value of the bulk modulus increases as a monotonic function of the nitrogen content from 298 GPa for bulk Tc to 341 GPa for the mechanically stable $P6_3/mmc$ TcN phase. The B values of Tc_3N (318 GPa) and Tc_2N (327 GPa) are 7% and 10% larger than the bulk Tc value, thus these materials are expected to possess enhanced hardness as they become more incompressible with increasing nitrogen content. However, these Tc nitrides phases are softer than their Re_3N (395 GPa) and Re_2N (401 GPa) congeners featuring strong Re–N covalent bonds.[10]

Similar to the recent findings reported for Re–N compounds,[37] B is systematically larger than G for all the Tc-bearing structures investigated, which suggests that the shear modulus is the parameter limiting the mechanical stability of the crystalline structures. The ratio $R_{G/B}$ of the shear modulus divided by the bulk modulus was proposed by Pugh as a simple indicator of the correlation between the ductile/brittle properties of metals and their elastic constants.[40] A material is considered ductile if $R_{G/B} < 0.5$, otherwise it is brittle. Therefore, all Tc compounds investigated here have a slightly ductile character with $R_{G/B}$ ranging from 0.45 for bulk Tc to 0.49 for the stable TcN phase.

The Cauchy pressure, C_{12}–C_{44}, which was suggested as a standard indicator of the angular character of atomic bonding, can also be related to the brittle/ductile properties of metals and metallic compounds.[41] Positive values of the Cauchy pressure are typically indicative of metallic bonding, while negative values correspond to directional bonding with angular character. The Cauchy pressure is positive for the bulk Tc (+67 GPa), Tc_3N (+38 GPa), Tc_2N (+12 GPa) and $P6_3/mmc$ TcN (+22 GPa) structures, indicating that metallic bonding is predominant.

As discussed by Frantsevich *et al.*,[42] the Poisson's ratio, ν, can also be utilized to measure the malleability of metals and metallic compounds and is related to the Pugh's ratio given above by the relation $R_{G/B} = (3 - 6\nu)/(8 + 2\nu)$. The Poisson's ratio is close to 1/3 for ductile materials, while it is generally much less than 1/3 for brittle materials. The computed Poisson's ratio for bulk Tc and Tc nitrides is in the range 0.29–0.30 and also points to a rather ductile character of these materials in the same way as $R_{G/B}$ and the Cauchy pressure.

Electronic structures

In order to understand the nature of the mechanical properties of Tc nitrides, their underlying electronic structure and bonding have been analyzed. Our calculations indicate that, like bulk Tc, these compounds are non-magnetic and feature metallic conductivity. Fig. 4 displays the computed total and orbital-projected densities of states (DOSs) of the bulk Tc, Tc_3N, Tc_2N and $P6_3/mmc$ TcN structures. In all Tc nitrides, valence and conduction bands near the Fermi level (E_F) are dominated by Tc 4d orbitals, which strongly hybridize with N 2p orbitals towards the bottom of the valence band to form covalent σ bonds. As the Tc/N

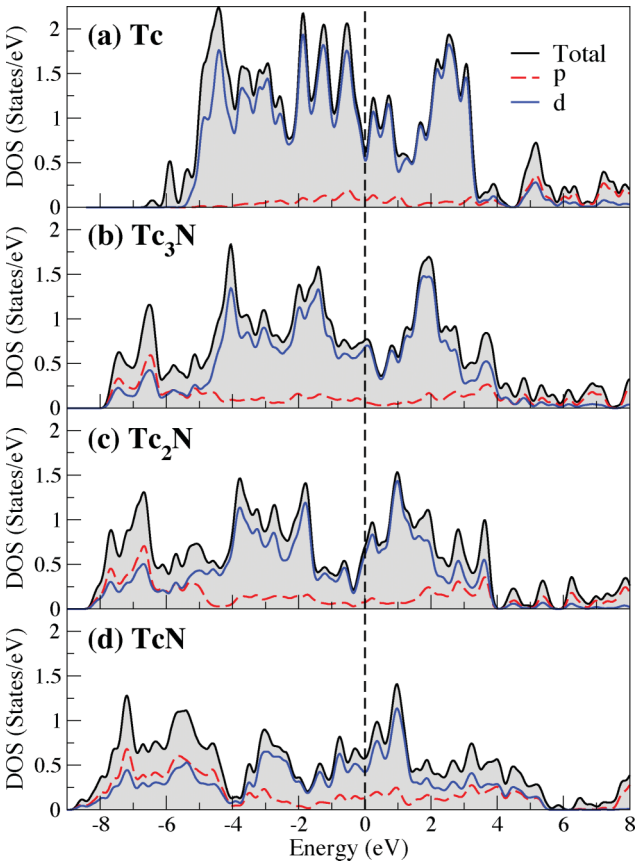

Fig. 4 Total and orbital-projected densities of states of (a) bulk Tc ($P6_3/mmc$), (b) Tc_3N ($P\bar{6}m2$), (c) Tc_2N ($P6_3/mmc$), and (b) TcN ($P6_3/mmc$) calculated at the GGA/PW91 level (in states/eV/atom). The Fermi energy is set to zero.

stoichiometry evolves from 3 : 1 to 1 : 1, the contribution of N 2p states below –4 eV becomes more important, resulting in more efficient hybridization with Tc 4d states and larger bulk modulus. However, the total DOS at E_F gradually decreases from 0.68 to 0.42 states/eV per atom from Tc_3N to TcN, accompanied by a reduction of the contribution of Tc 4d states to the total DOS from 89% to 72% at the Fermi level, thus suggesting an appreciable deterioration of metallic conductivity with increasing N content. This finding is consistent with the overall variation in metallic character from Tc_3N to TcN indicated by the Cauchy pressure.

Partial charges calculated using the Mulliken partitioning of the electron density were also analyzed for Tc nitrides. While the charge carried by N remains essentially identical in all Tc nitrides (≈ –0.72 *e*), the charge of Tc atoms varies monotonically, *i.e.* +0.22 and +0.25 *e* on Tc atoms at 1*f* and 2*h* positions in Tc_3N, +0.36 *e* in Tc_2N, and +0.73 *e* in TcN. This Tc→N charge transfer points to a growing degree of ionic character with increasing N content in Tc compounds.

Electron charge density maps of the $(11\bar{2}0)$ plane of bulk Tc, Tc_3N, Tc_2N, and $P6_3/mmc$ TcN in Fig. 5 show directional Tc–Tc and Tc–N bonds resulting from the delocalized metallic-type interaction between Tc 4d states near E_F and from the strong hybridization of Tc 4d–N 2p states, respectively. As depicted in Fig. 5(d), the aforementioned difference of +0.03 *e* between Mulliken charges of Tc atoms at 1*f* and 2*h* positions in Tc_3N can be explained

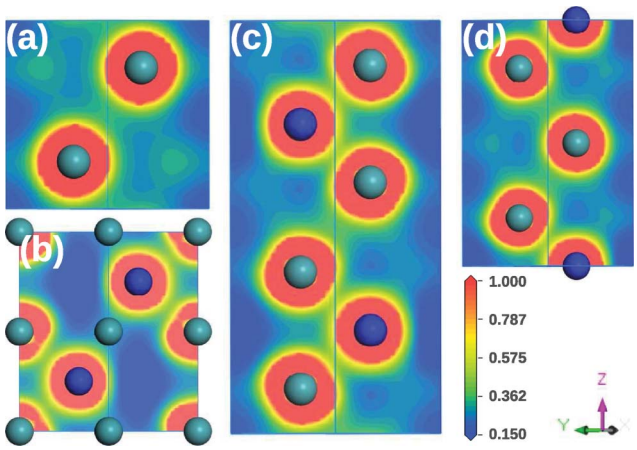

Fig. 5 Cross-sectional views of the electron charge density in the (11$\bar{2}$0) plane of (a) bulk Tc ($P6_3/mmc$), (b) TcN ($P6_3/mmc$), (c) Tc_2N ($P6_3/mmc$), and (d) Tc_3N ($P\bar{6}m2$) structures calculated at the GGA/PW91 level. Charge densities are plotted in e Å^{-3}. Color legend: N, navy blue; Tc, grey.

by the proximity of N atoms near Tc at 2*h* positions. This leads to enhanced Tc(2*h*)→N charge transfer and a larger positive Tc(2*h*) charge compared to the Tc(1*f*) involved only in Tc–Tc bonds.

Conclusions

We have studied the structures and properties of technetium nitride phases within the framework of gradient-corrected density functional theory. Our results indicate that novel Tc_3N and Tc_2N subnitrides crystallizing in the $P\bar{6}m2$ and $P6_3/mmc$ space groups, respectively, are mechanically stable. Calculations of the enthalpy of formation in the athermal limit reveal a propensity of the TcN system to form Tc-rich phases rather than stoichiometric TcN. The computed value of the bulk modulus increases as a monotonic function of the nitrogen content from 298 GPa for bulk Tc to 341 GPa for the mechanically stable $P6_3/mmc$ TcN phase, thus these materials are expected to possess enhanced hardness as they become more incompressible with increasing nitrogen content. These compounds are also predicted to be slightly ductile and possess a dominant metallic character. Density of states calculations and charge analysis show that a complex mixture of metallic, ionic, and covalent contributions stems from the formation of directional Tc–Tc and Tc–N bonds resulting from the delocalized metallic-type interaction between Tc 4d states near E_F and from the strong hybridization of Tc 4d–N 2p states, respectively.

Computational Methods

First-principles total energy calculations were performed using spin-polarized density functional theory, as implemented in the Vienna *Ab initio* Simulation Package (VASP)[43] and in the CASTEP code.[44] The exchange–correlation energy was calculated using the generalized gradient approximation[45] (GGA) with the parametrization of Perdew and Wang[46] (PW91). For structures bearing transition metals, pure functionals such as the PW91 are generally preferred over hybrid functionals that appear to describe metal–metal bonds less accurately.[47,48] In particular, the PW91 functional was found to correctly describe the geometric parameters and properties of various Tc-containing structures.[49–53]

In the VASP calculations, the interaction between valence electrons and ionic cores was described by the Projector Augmented Wave (PAW) method.[54,55] The Tc $4p^6 5s^2 4d^5$ and N $2s^2 2p^3$ electrons were treated explicitly as valence electrons in the Kohn–Sham (KS) equations and the remaining cores were represented by PAW pseudopotentials. The KS equations were solved using the blocked Davidson iterative matrix diagonalization scheme followed by the residual vector minimization method. The plane-wave cutoff energy for the electronic wavefunctions was set to 500 eV. Crystal structures were optimized with periodic boundary conditions applied using the conjugate gradient method, accelerated using the Methfessel–Paxton Fermi-level smearing[56] with a Gaussian width of 0.1 eV. The total energy of the molecular system and Hellmann–Feynman forces acting on atoms were calculated with convergence tolerances set to 10^{-3} eV and 0.01 eV Å^{-1}, respectively.

In the CASTEP calculations, norm-conserving pseudopotentials were used to represent the interaction between valence electrons and ions, with a plane-wave cutoff energy set to 770 eV. The Broyden-Fletcher-Goldfarb-Shanno (BFGS) method was used for geometry optimization with convergence tolerances for the total energy, maximum ionic force, maximum ionic displacement, and maximum stress components fixed to 5×10^{-6} eV/atom, 0.01 eV Å^{-1}, 5×10^{-4} Å, and 0.02 GPa, respectively.

All structural optimizations and properties calculations were carried out using the Monkhorst–Pack special k-point scheme[57] with 11 × 11 × 11 and 11 × 11 × 7 meshes for integrations in the Brillouin zone (BZ) of cubic and hexagonal systems, respectively. For bulk Tc, the HCP (space group $P6_3/mmc$, Z = 2) and FCC (space group $Fm\bar{3}m$, Z = 4) structures observed experimentally were investigated. For Tc mononitride, candidate phases crystallizing in the NaCl (space group $Fm\bar{3}m$, Z = 4), NiAs (space group $P6_3/mmc$, Z = 2), WC (space group $P\bar{6}m2$, Z = 1), wurtzite-type ZnS (space group $P6_3mc$, Z = 2), and zincblende-type ZnS (space group $F\bar{4}3m$, Z = 4) structures were studied. For Tc subnitrides, the Tc_3N (space group $P\bar{6}m2$, Z = 1) and Tc_2N (space group $P6_3/mmc$, Z = 2) analogues of the recently discovered stoichiometric Re nitrides were considered.[10] For hexagonal structures, the c/a ratio optimization of the lattice parameters was performed at constant volume.

Considering the following reaction to form crystalline bulk Tc nitrides from the elements in the athermal limit,

$$\mathrm{Tc} + \frac{1}{2}\mathrm{N_2(s)} \rightarrow \mathrm{Tc}_x\mathrm{N}, \quad (1)$$

the enthalpy of formation at 0 K was computed using the expression:

$$\Delta H_f = E_{\mathrm{tot}}^{\mathrm{Tc}_x\mathrm{N}} - E_{\mathrm{tot}}^{\mathrm{Tc}} - (1/2)E_{\mathrm{tot}}^{\mathrm{N_2(s)}}, \quad (2)$$

where $E_{\mathrm{tot}}^{\mathrm{TcxN}}$, $E_{\mathrm{tot}}^{\mathrm{N2\,(s)}}$, and $E_{\mathrm{tot}}^{\mathrm{Tc}}$ are the total energies of the bulk Tc nitride system (x = 1–3), the α phase of N_2 molecular solid,[58] and the bulk HCP Tc, respectively.

Strains and stresses necessary to obtain the full 6 × 6 stiffness tensor of elastic constants, C_{ij}, were computed using the crystal structures relaxed with CASTEP. Elastic constants were further used to calculate the bulk modulus, B, and the shear modulus,

G, within the Voigt[59] and Reuss[60] approximations. For cubic structures with three independent elastic constants C_{11}, C_{44} and C_{12}, they can be evaluated using the formulas:

$$B_V = B_R = (C_{11} + C_{12})/3,$$

$$G_V = (C_{11} + C_{12})/5,$$

$$G_R = 5C_{44}(C_{11} + C_{12})/[4C_{44} + 3(C_{11} - C_{12})],$$

where the V and R subscripts denote the Voigt and Reuss bounds. For hexagonal structure with five independent elastic constants C_{11}, C_{33}, C_{44}, C_{12} and C_{13}, they can be obtained from the expressions:

$$B_V = [2(C_{11} + C_{12}) + 4C_{13} + C_{33}]/9,$$

$$B_R = C^2/M,$$

$$G_V = (M + 12C_{44} + 12C_{66})/30,$$

$$G_R = (5/2)C^2C_{44}C_{66}/[3B_VC_{44}C_{66} + C^2(C_{44} + C_{66})],$$

where $C_{66} = (C_{11} - C_{12})/2$, $M = C_{11} + C_{12} + 2C_{33}–4C_{13}$, $C^2 = (C_{11} + C_{12})C_{33} - 2C^2_{13}$.

For the sake of comparison with the Re_3N and Re_2N subnitrides recently synthesized as polycrystalline species,[10] the effective moduli for isotropic polycrystals were calculated within the Voigt-Reuss-Hill's (VRH) approximation[61] as the averaged Voigt and Reuss limits, *i.e.* $B_H \equiv B = (B_R + B_V)/2$ and $G_H \equiv G = (G_R + G_V)/2$. The averaged compressibility, β, Young's modulus, E, and Poisson's ratio, ν, were derived from the formulas:

$$\beta = 1/B,$$

$$E = 9BG/(3B + G),$$

$$\nu = (1/2)(3B - 2G)/(3B + G).$$

Acknowledgements

This project was funded under the auspices of the U.S. Department of Energy, Office of Nuclear Energy, Cooperative Agreement No. DE-FG07-01AL67358. Funding for this research was also provided by a subcontract through Battelle 0089445 from the U.S. Department of Energy, Agreement No. DE-AC07-05ID14517.

References

1 L. E. Toth, *Transition Metal Carbides and Nitrides*, Academic Press, New York, 1971.
2 S. H. Jhi, J. Ihm, S. G. Louie and M. L. Cohen, *Nature*, 1999, **399**, 132.
3 P. F. McMillan, *Nat. Mater.*, 2002, **1**, 19.
4 A. Zerr, G. Miehe and R. Riedel, *Nat. Mater.*, 2003, **2**, 185.
5 M. Chhowalla and H. E. Unalan, *Nat. Mater.*, 2005, **4**, 317.
6 R. B. Kaner, J. J. Gilman and S. H. Tolbert, *Science*, 2005, **308**, 1268.
7 E. Gregoryanz, C. Sanloup, M. Somayazulu, J. Badro, G. Fiquet, H. K. Mao and R. J. Hemley, *Nat. Mater.*, 2004, **3**, 294.
8 J. C. Crowhurst, A. F. Goncharov, B. Sadigh, C. L. Evans, P. G. Morrall, J. L. Ferreira and A. J. Nelson, *Science*, 2006, **311**, 1275.
9 A. F. Young, C. Sanloup, E. Gregoryanz, S. Scandolo, R. J. Hemley and H. K. Mao, *Phys. Rev. Lett.*, 2006, **96**, 155501.
10 A. Friedrich, B. Winkler, L. Bayarjargal, W. Morgenroth, E. A. Juarez-Arellano, V. Milman, K. Refson, M. Kunz and K. Chen, *Phys. Rev. Lett.*, 2010, **105**, 085504.
11 D. Åberg, P. Erhart, J. Crowhurst, J. M. Zaug, A. F. Goncharov and B. Sadigh, *Phys. Rev. B: Condens. Matter Mater. Phys.*, 2010, **82**, 104116.
12 O. N. Pierson, *Handbook of Refractory Carbides and Nitrides. Properties, Characteristics, Processing and Applications*, Noyes Publications, New Jersey, 1996.
13 R. Yu, Q. Zhan and L. C. De Jonghe, *Angew. Chem., Int. Ed.*, 2007, **46**, 1136.
14 H. Hahn and A. Konrad, *Z. Anorg. Allg. Chem.*, 1951, **264**, 174.
15 A. U. Haq and O. Meyer, *J. Low Temp. Phys.*, 1983, **50**, 123.
16 P. Clark, B. Dhandapani and S. T. Oyama, *Appl. Catal., A*, 1999, **184**, L175.
17 R. Kojima and K.-I. Aika, *Appl. Catal., A*, 2001, **209**, 317.
18 G. Soto, A. Rosas, M. H. Farias, W. De la Cruz and J. A. Diaz, *Mater. Charact.*, 2007, **58**, 519.
19 M. Fuchigami, K. Inumaru and S. Yamanaka, *J. Alloys Compd.*, 2009, **486**, 621.
20 W. Trzebiatowski and J. Rudzinski, *J. Less Common Met.*, 1964, **6**, 244.
21 I. V. Vinogradov, M. I. Konarev, L. L. Zaitseva and S. V. Shepel'kov, *Russ. J. Inorg. Chem.*, 1978, **23**, 977.
22 K. H. Lieser, *Radiochim. Acta*, 1993, **63**, 5.
23 A. Maes, K. Geraedts, C. Bruggeman, J. Vancluysen, A. Rossberg and C. Hennig, *Environ. Sci. Technol.*, 2004, **38**, 2044.
24 R. Pasqualini, V. Comazzi, E. Bellande, A. Duatti and A. Marchi, *Int. J. Radiat. Appl. Instrum., Part A*, 1992, **43**, 1329.
25 K. Schwochau, *Technetium: Chemistry and Radiopharmaceutical Applications*, Wiley-VHC, New York, 2000.
26 T. Storr, K. H. Thompson and C. Orvig, *Chem. Soc. Rev.*, 2006, **35**, 534.
27 F. Tisato, M. Porchia, C. Bolzati, F. Refosco and A. Vittadini, *Coord. Chem. Rev.*, 2006, **250**, 2034.
28 C. Bolzati, M. Cavazza-Ceccato, S. Agostini, F. Tisato and G. Bandoli, *Inorg. Chem.*, 2008, **47**, 11972.
29 A. Fernández Guillermet, J. Häglund and G. Grimvall, *Phys. Rev. B: Condens. Matter*, 1992, **45**, 11557.
30 R. de Paiva, R. A. Nogueira and J. L. A. Alves, *Phys. Rev. B: Condens. Matter Mater. Phys.*, 2007, **75**, 085105.
31 C. S. Barrett and T. B. Massalski, *Structure of Metals*, Pergamon, New York, 1980.
32 J. A. Rard, M. H. Rand, G. Andregg and H. Wanner, in *Chemical Thermodynamics, vol. 3: Chemical Thermodynamics of Technetium*, M. C. A. Sandino and E. Osthols, ed., Issy-les-Moulineaux (France), OECD Nuclear Energy Agency, Data Bank, 1999.
33 V. M. Golyanov, L. A. Elesin and N. M. Mikheeva, *Zh. Eksp. Teor. Fiz.*, 1973, **18**, 572.
34 D. A. Young, *Phase Diagrams of the Elements*, UC Press, Berkeley, 1976, p. 176.
35 M. Born and K Huang, *Dynamical Theory of Crystal Lattices*, Clarendon, Oxford, 1956.
36 A. Fernández-Guillemet and G. Grimvall, *J. Less Common Met.*, 1989, **147**, 195.
37 V. V. Bannikov, I. R. Shein, A. L. Ivanovskii, http://arxiv.org/pdf/1011.3932.
38 P. Ravindran, L. Fast, P. A. Korzhavyi, B. Johansson, J. Wills and O. Eriksson, *J. Appl. Phys.*, 1998, **84**, 4891.
39 S. I. Ranganathan and M. Ostoja-Starzewski, *Phys. Rev. Lett.*, 2008, **101**, 055504.
40 S. F. Pugh, *Philos. Mag.*, 1954, **45**, 823.
41 D. G. Pettifor, *Mater. Sci. Technol.*, 1992, **8**, 345.
42 I. N. Frantsevich, F. F. Voronov and S. A. Bokuta, *Elastic Constants and Elastic Moduli of Metals and Insulators Handbook*, I. N. Frantsevich Ed., Naukova Dumka, Kiev, 1983, pp. 60–180.
43 G. Kresse and J. Furthmüller, *Phys. Rev. B: Condens. Matter*, 1996, **54**, 11169.
44 S. J. Clark, M. D. Segall, C. J. Pickard, P. J. Hasnip, M. J. Probert, K. Refson and M. C. Payne, *Z. Kristallogr.*, 2005, **220**, 567.
45 J. P. Perdew, J. A. Chevary, S. H. Vosko, K. A. Jackson, M. R. Pederson, D. J. Singh and C. Fiolhais, *Phys. Rev. B: Condens. Matter*, 1992, **46**, 6671.
46 J. P. Perdew and Y. Wang, *Phys. Rev. B: Condens. Matter*, 1992, **45**, 13244.
47 G. L. Gutsev and C. W. Bauschlicher, *J. Phys. Chem. A*, 2003, **107**, 7013.

48 F. Furche and J. P. Perdew, *J. Chem. Phys.*, 2006, **124**, 044103.
49 P. F. Weck, E. Kim, F. Poineau, E. E. Rodriguez, A. P. Sattelberger and K. R. Czerwinski, *Inorg. Chem.*, 2009, **48**, 6555.
50 P. F. Weck, E. Kim, F. Poineau and K. R. Czerwinski, *Phys. Chem. Chem. Phys.*, 2009, **11**, 10003.
51 P. F. Weck, E. Kim, F. Poineau, E. E. Rodriguez, A. P. Sattelberger and K. R. Czerwinski, *Dalton Trans.*, 2010, **39**, 7207.
52 P. F. Weck, E. Kim, K. R. Czerwinski and D. Tománek, *Phys. Rev. B: Condens. Matter Mater. Phys.*, 2010, **81**, 125448.
53 P. F. Weck, A. P. Sergeeva, E. Kim, A. I. Boldyrev and K. R. Czerwinski, *Inorg. Chem.*, 2011, **50**, 1039.
54 P. E. Blöchl, *Phys. Rev. B: Condens. Matter*, 1994, **50**, 17953.
55 G. Kresse and D. Joubert, *Phys. Rev. B: Condens. Matter Mater. Phys.*, 1999, **59**, 1758.
56 M. Methfessel and A. T. Paxton, *Phys. Rev. B*, 1989, **40**, 3616.
57 H. J. Monkhorst and J. D. Pack, *Phys. Rev. B: Solid State*, 1976, **13**, 5188.
58 J. A. Venables and C. A. English, *Acta Crystallogr., Sect. B: Struct. Crystallogr. Cryst. Chem.*, 1974, **30**, 929.
59 W. Voigt, *Lehrburch der Kristallphysik*, Teubner, Leipzig, 1928.
60 A. Reuss, *Z. Angew. Math. Mech.*, 1929, **9**, 49.
61 R. Hill, *Proc. Phys. Soc. Lond.*, 1952, **65**, 350.

